ACS Photonics

pubs.acs.org/journal/apchd5

Article

Surface-Enhanced Circular Dichroism Spectroscopy on Periodic Dual Nanostructures

Jon Lasa-Alonso,* Diego Romero Abujetas, Álvaro Nodar, Jennifer A. Dionne, Juan José Sáenz, Gabriel Molina-Terriza, Javier Aizpurua, and Aitzol García-Etxarri*

Cite This: https://dx.doi.org/10.1021/acsphotonics.0c00611

Read Online

ACCESS | Metrics & More | Article Recommendations | Supporting Information

ABSTRACT: Increasing the sensitivity of chiral spectroscopic techniques such as circular dichroism (CD) spectroscopy is a current aspiration in the research field of nanophotonics. Enhancing CD spectroscopy depends on two complementary requirements: the enhancement of the electromagnetic fields perceived by the molecules under study and the conservation of the helicity of those fields, guaranteed by duality symmetry. In this work, we introduce a systematic method to design nanostructured dual periodic photonic systems capable of enhancing molecular CD spectroscopy resonantly. As an illustration, we engineer a dual 1D silicon nanoparticle array and show that its collective optical modes can be efficiently employed to resonantly enhance by 2 orders of magnitude the local density of optical chirality and, thus, the CD signal obtained from a given molecular sample on its vicinity.

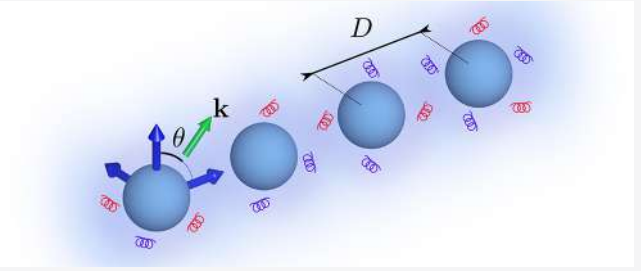

KEYWORDS: *circular dichroism, chirality, duality symmetry, lattice resonances, high refractive index nanoparticles*

Circular dichroism (CD) spectroscopy is a widely used experimental technique that enables the characterization of chiral molecular samples. This technique, which measures the differential absorption of molecules to left- and right-handed circularly polarized light (CPL) excitation, permits, for instance, the characterization of the secondary structure of biomolecules and to determine the enantiopurity of pharmaceutical drugs.[1] Despite its wide applicability, the sensitivity of CD measurements is quite limited due to the weak nature of chiral light−matter interactions. Nanostructured materials have been instrumental in enhancing the sensitivity of other molecular spectroscopic techniques such as Surface-Enhanced Raman Scattering (SERS) and Surface-Enhanced Infrared Absorption (SEIRA) spectroscopy, increasing their performance several orders of magnitude.[2−6] Similarly, increasing the sensitivity of CD spectroscopy with the aid of nanostructures would be highly desirable and it is a research objective that has been pursued in the recent past.

Since the seminal contributions of Y. Tang and A. E. Cohen,[7] several nanophotonic platforms have been proposed to augment the sensitivity of CD experiments through the local and global enhancement of $C(\mathbf{r})$, the local density of electromagnetic chirality. To mention a few, high refractive index nanoparticles,[8−13] plasmonic chiral[14,15] and nonchiral nanoantennas,[15−17] optical waveguides,[18] and metasurfaces[19−22] have been explored as enablers of surface-enhanced circular dichroism and other chiral spectroscopy techniques.

Globally enhancing CD spectroscopy around a nanostructure necessitates duality symmetry[23] in the design of the device so that the helicity of the scattered fields is conserved. Unfortunately, common nanophotonic platforms can only guarantee this symmetry at particular, nonresonant, excitation wavelengths or, alternatively, under certain illumination conditions. This limits the efficiency of light−matter interactions between the scattered fields and the molecules under study, limiting the magnitude of the achievable enhancements in CD spectroscopy.

In this work, we present a novel approach to design helicity preserving and optically resonant nanostructured devices to enhance the CD signal, exploiting the lattice modes of periodic arrays of dual high refractive index nanoparticles. Starting from the well-known example of a silicon nanosphere capable of enhancing the CD spectroscopy signal by a factor of 10,[8] we first characterize the resonances of a 1D array of such nanoparticles. We observe that these systems support at least two different types of emerging lattice resonances: far-field diffractive modes and a nondiffractive lattice resonance mediated by mid- and near-field interactions. In addition, we find that, in finite particle arrays, finite chain effects can also be observed and exploited.

Received: April 15, 2020

We show that these helicity preserving resonant modes can globally enhance the sensitivity of CD spectroscopy over 2 orders of magnitude, providing one additional order of magnitude enhancement over the response of a single, nonresonant nanoparticle.[8] Moreover, the spherical geometry of our lattice components allows us to observe consistent enhancements for CD at any angle of incidence. Although the maximum enhancement is given for the far-field diffractive modes, we also find that enhancements obtained in the rest of the cases are comparable.

Enhanced Chiral Light−Matter Interactions and Helicity Conservation. For molecules illuminated by a left- (+) or right-handed (-) circularly polarized plane wave in vacuum, the CD signal of a molecule, CD_{cpl}, can be expressed as[7,8]

$$CD_{cpl} = -\frac{4}{\varepsilon_0}\mathrm{Im}(G)|C_{cpl}| \tag{1}$$

where G is the molecular chiral polarizability, $C_{cpl} = \pm\frac{\varepsilon_0\omega}{2c}E_0^2$ is the local density of chirality of a plane wave in vacuum, c is the speed of light, ω is the angular frequency, E_0 is the amplitude of the incoming electric field, and ε_0 is the permittivity of free space. Reference 8 concluded that, in the presence of nonchiral antennas, the CD signal could be locally expressed as

$$CD(\mathbf{r}) = -\frac{4}{\varepsilon_0}\mathrm{Im}(G)C(\mathbf{r}) \tag{2}$$

with $C(\mathbf{r}) = -\frac{\omega}{2c^2}\mathrm{Im}(\mathbf{E}(\mathbf{r})^*\cdot\mathbf{H}(\mathbf{r}))$ being the local density of optical chirality,[7] where $\mathbf{E}(\mathbf{r})$ and $\mathbf{H}(\mathbf{r})$ are the local electric and magnetic fields, respectively. Although G is a fixed molecular parameter, $C(\mathbf{r})$ can be, in principle, engineered and enhanced in the presence of optical antennas. Importantly, in the presence of nonchiral antennas, one can define a local enhancement factor such that $CD(\mathbf{r}) = f_{CD(\mathbf{r})}CD_{cpl}$, where

$$f_{CD(\mathbf{r})} = \frac{CD(\mathbf{r})}{CD_{cpl}} = \frac{C(\mathbf{r})}{|C_{cpl}|} = -\frac{Z_0}{E_0^2}\mathrm{Im}(\mathbf{E}(\mathbf{r})^*\cdot\mathbf{H}(\mathbf{r})) \tag{3}$$

Z_0 being the impedance of vacuum.

Contrary to what could be intuitively expected, the local density of chirality, $C(\mathbf{r})$, is not necessarily related to the local handedness of the field. Nevertheless, as shown in eq 2, the CD signal is directly proportional to $C(\mathbf{r})$ in the presence of nonchiral environments. Therefore, an essential element to enhance the CD signal is to engineer the local fields, so that the overall sign of $C(\mathbf{r})$ (and, thus, also the sign of $f_{CD(\mathbf{r})}$) is preserved, while its magnitude is maximized. Our work is focused on finding a nanostructure which, when illuminated by CPL of a given handedness, can enhance the absolute value of $C(\mathbf{r})$ while locally preserving its sign in space. In such a scenario, molecules in the vicinity of our optical resonator will interact with the local field in a way that always contributes favorably to the CD signal. This allows for a strict spatial control on the molecular absorption rates and facilitates the practical measurement of the field-enhanced CD signal.

In the case of monochromatic fields, the electromagnetic density of chirality is intimately related to the local density of helicity.[24−27] The helicity operator can be expressed as

$$\Lambda = \frac{\mathbf{J}\cdot\mathbf{P}}{|\mathbf{P}|} = \frac{1}{k}\nabla\times \tag{4}$$

where $\mathbf{J}$ is the total angular momentum of light, $\mathbf{P}$ is the linear momentum, and the second equality in eq 4 is only held for monochromatic fields.[28] The helicity operator is the generator of dual transformations, that is, rotations of the electric and magnetic fields.[23] Hence, the helicity is a conserved magnitude in the interaction of light with systems symmetric under the exchange of electric and magnetic fields, the so-called dual systems (for an in-depth discussion about electromagnetic duality symmetry and helicity conservation, we refer the reader to some key references in the field[23,29−31]).

In single particles with a dominant dipolar response, duality symmetry is fulfilled for wavelengths that meet the first Kerker's condition, in other words, for wavelengths where the electric and magnetic polarizabilities of the nanostructure are equal ($\alpha_e = \alpha_m$).[29,32−36] This condition can be achieved for particular wavelengths of light and materials.[37] Similarly, in a collection of nanoparticles, duality is a symmetry of the whole system if every individual particle satisfies the first Kerker's condition.[23,30]

When duality symmetry is fulfilled in such scenarios, the helicity eigenstates play an important role in the dynamics of the interaction, as they are conserved. Helicity eigenstates have interesting properties as can be seen in the following expressions for the local electric and magnetic fields[30]

$$\Lambda\mathbf{E}(\mathbf{r}) = \frac{1}{k}\nabla\times\mathbf{E}(\mathbf{r}) = p\mathbf{E}(\mathbf{r}) \tag{5}$$

$$\Lambda\mathbf{H}(\mathbf{r}) = \frac{1}{k}\nabla\times\mathbf{H}(\mathbf{r}) = p\mathbf{H}(\mathbf{r}) \tag{6}$$

where the helicity eigenvalue is $p = \pm 1$. Maxwell's equations also relate the second equality from eq 5 with the magnetic field and, conversely, eq 6 with the electric field. Then, for helicity eigenstates, one obtains $\mathbf{H}(\mathbf{r}) = \frac{-ipk}{\omega\mu_0}\mathbf{E}(\mathbf{r})$. Applying this expression to eq 3, the local CD enhancement factor for dual systems can be reformulated as

$$f_{CD}^{dual(\mathbf{r})} = \frac{1}{E_0^2}|\mathbf{E}(\mathbf{r})|^2 \tag{7}$$

For dual systems helicity eigenstates do not mix, i.e. helicity is a conserved quantity. Then, on the one hand, eq 7 confirms that under duality symmetry, $C(\mathbf{r})$ does not change sign locally upon scattering. Most importantly, this result predicts that we can enhance the local CD experimental signal on a dual structure as far as we are able to enhance the fields close to our optical system. Finally, this expression comes into agreement with other results in the literature, which express the chirality in terms of the Riemann-Silberstein vectors.[13,38]

Lattice Resonances. As we determined in the previous section, dual systems allow for the enhancement of $f_{CD(\mathbf{r})}$ while keeping its local sign unaltered. Nevertheless, duality symmetry constriction restricts the chirality enhancement to specific wavelengths which fulfill Kerker's first condition. Importantly, if dual behavior is sought, regardless of the direction of the incoming beam, this wavelength does not typically coincide with resonant modes of isotropic optical cavities and resonators. As a consequence, the electromagnetic fields used in typical surface-enhanced CD devices are not usually very intense on isolated nanoparticles. Previous results for isotropic high refractive index single nanoparticles[8] predict a modest enhancement of 1 order of magnitude in the molecular CD signal. In order to overcome this limitation, we propose to

https://dx.doi.org/10.1021/acsphotonics.0c00611
ACS Photonics XXXX, XXX, XXX−XXX

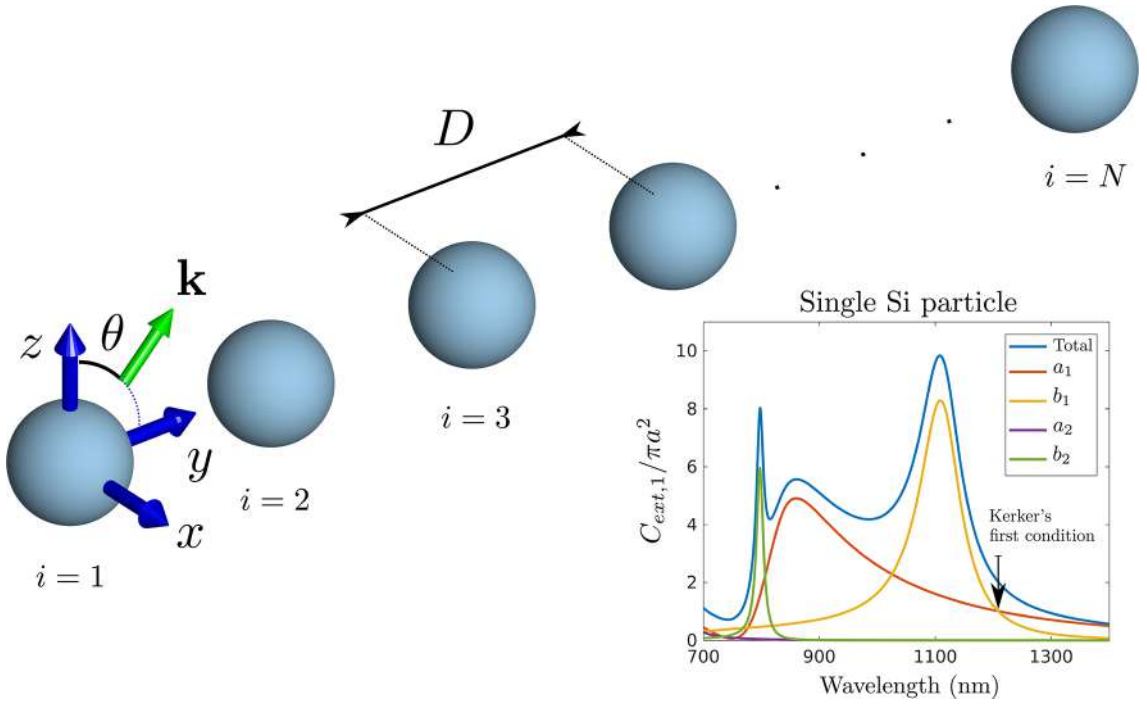

Figure 1. Sketch of the setup under study: a group of nanoparticles arranged in a 1D periodic arrangement. In the inset, the extinction cross section of a single isolated silicon nanoparticle with radius a = 150 nm is shown. Palik's experimental data[39] has been used for the refractive index. In the legend, a_1 refers to the electric dipole, b_1 to the magnetic dipole, a_2 to the electric quadrupole, and b_2 to the magnetic quadrupole contributions to the extinction cross section.

exploit lattice resonances arising in ordered collections of dual, nonresonant, individual dielectric nanoparticles. For the sake of clarity, we restrict our study to 1D periodic arrangements of silicon nanoparticles. Nevertheless, ideas presented in this article can be easily generalized for 2D or 3D particle arrays.

Lattice resonances are collective excitations of periodically arranged groups of nanoparticles. Equation 7 indicates that, on any dual system, $f_{CD}^{dual(r)}$ scales with the square of the field enhancement that is produced. Thus, our hypothesis is that although the individual nanoparticles are nonresonant at the first Kerker's condition, their collective behavior at particular separation distances can give rise to resonant, very intense, circularly polarized fields capable of uniformly enhancing the CD spectroscopic signal of molecules over the entire extension of the array. Thus, in order to guarantee duality symmetry, we will operate at a particular frequency at which Kerker's first condition is fulfilled by every particle in the lattice, while we modify the separation distance between them to induce a resonant behavior of the periodic system. It is important to point out that fulfilling Kerker's first condition is independent of the position of the spheres in the array. In other words, if duality symmetry is restored for a given piecewise inhomogeneous medium, it will also be restored if the domains of such a medium are spatially rearranged (see Supporting Information).[23]

In the small particle limit, the optical response of each nanoparticle can be described as a combination of a point electric dipole and a point magnetic dipole. The inset in Figure 1 shows that, in the first Kerker's condition (λ_k = 1208 nm), the magnitude of the electric (a_2) and magnetic (b_2) quadrupole is negligible compared to the electric (a_1) and magnetic (b_1) dipolar contributions. Thus, in such situations, the collective behavior of the system can be analyzed using an approach based on the Coupled Dipole Approximation (CDA). For a finite collection of N particles, the optical response of the coupled electric and magnetic dipoles has a well-known algebraic solution:

$$\vec{\Psi} = [\boldsymbol{I} - k^2 \boldsymbol{G}_F \boldsymbol{\alpha}_F]^{-1} \vec{\Psi}_0 \tag{8}$$

$\vec{\Psi}$ is a $6N$ dimensional vector that contains the self-consistent solution for each electric and magnetic field components in every site. $\boldsymbol{I}$ is the $6N \times 6N$ identity matrix and $\boldsymbol{\alpha}_F$ is a matrix of the same size containing the values of the electric and magnetic polarizabilities. $\boldsymbol{G}_F$ is a matrix that contains the coupling coefficients (built as lattice sums of Green's functions) between all the different dipoles in the system. Finally, $\vec{\Psi}_0$ is a $6N$ dimensional vector containing the values of the incident electric and magnetic fields at each of the positions of the particles (more detailed information can be found in the Supporting Information).

Collective resonances emerge when $\det(\boldsymbol{I} - k^2 \boldsymbol{G}_F \boldsymbol{\alpha}_F) \approx 0$ (notice that real poles would signal the existence of bound states). In these situations, the scattered fields around the nanoparticles are strongly enhanced and, thus, $f_{CD(r)}$ increases substantially. Note that since the incident wavelength and, therefore, the polarizabilities of the particles are fixed to fulfill duality symmetry, the emergence of collective modes depends only on geometrical values, namely, the spatial distribution of the nanoparticles and the direction of incidence of the probing CPL.

It is also important to note that there are different interaction mechanisms through which nanoparticles can interact in a periodic structure to give rise to collective resonances. On the one hand, if the photonic elements are placed at relatively long separation distances, they interact through a r^{-1} dependent far-field dipolar interaction giving rise

https://dx.doi.org/10.1021/acsphotonics.0c00611
ACS Photonics XXXX, XXX, XXX−XXX

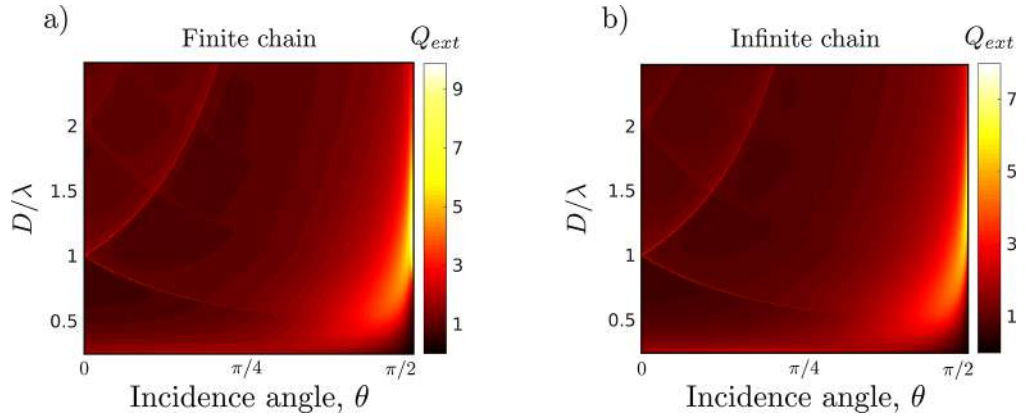

Figure 2. Normalized extinction cross section map under Kerker's first condition ($\lambda = \lambda_k$) as a function of interparticle distance for (a) a finite periodic 1D array of 2000 silicon nanospheres and (b) an infinitely periodic 1D array of silicon nanospheres.

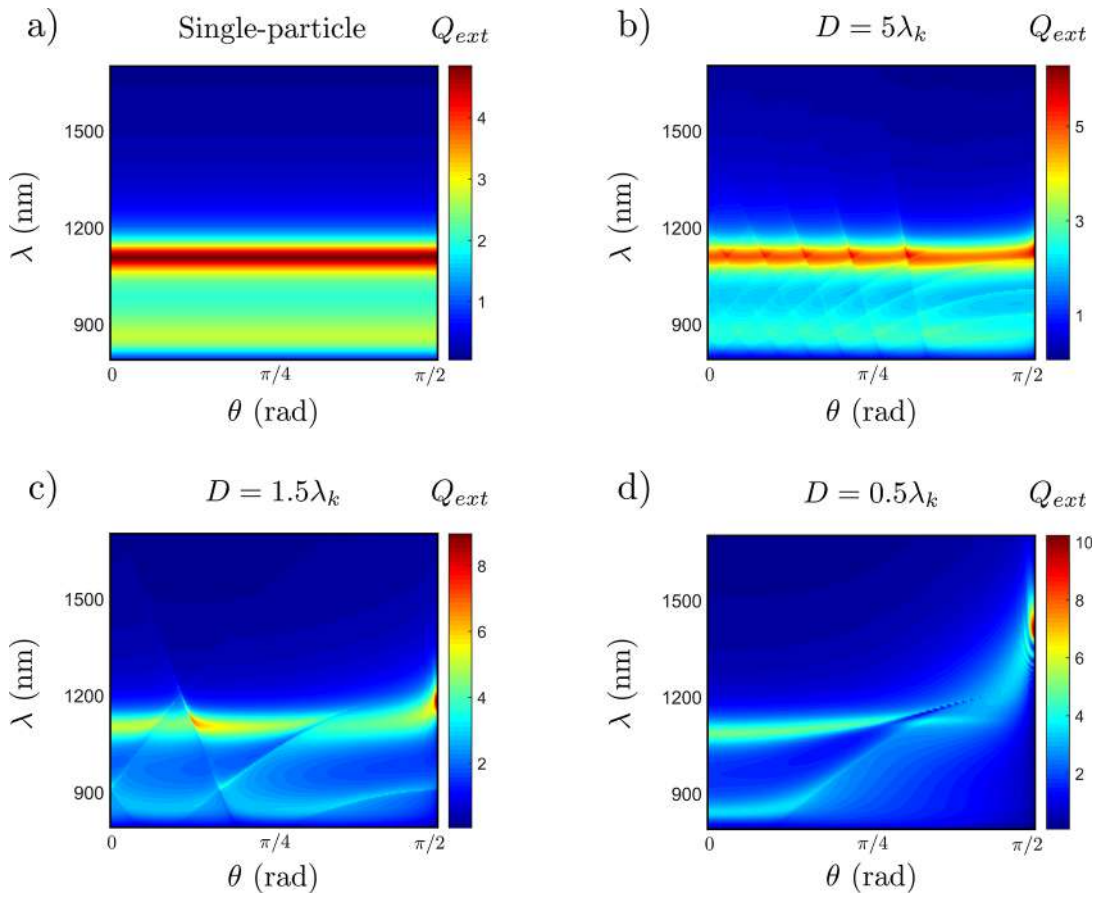

Figure 3. Normalized extinction cross section map as a function of the illuminating wavelength for (a) a single silicon nanosphere, (b) a chain of 2000 nanospheres with $D = 5\lambda_k$, (c) a chain of 2000 nanospheres with $D = 1.5\lambda_k$, and (d) a chain of 2000 nanospheres with $D = 0.5\lambda_k$.

to high-quality factor diffractive modes.[40] On the other hand, if the particles are more closely spaced, r^{-3} and r^{-2} dependent near-field interactions can also give rise to broader hybridized chain modes.[41,42]

In what follows, we show that lattice resonances based on both types of interaction mechanisms are, in practice, useful to enhance the local density of optical chirality $C(\mathbf{r})$ and, thus, enhance the CD signal, setting a useful photonic paradigm for experimental testing. We have chosen our proof-of-concept system to be a finite 1D array of silicon dual nanoparticles showing that both types of lattice resonances give rise to an important enhancement of $f_{CD(\mathbf{r})}$.

Finite Chain of Dual Nanospheres. In the following, we study a 1D array of $N = 2000$ silicon nanospheres of radius $a = 150$ nm located along the OY axis such that the nanospheres are placed at $\mathbf{r}_i = (i-1)D\hat{\mathbf{u}}_y$, where $i = 1, 2, ..., N$ and D is the distance between two adjacent nanoparticles from center to center. In addition, the wavevector $(\mathbf{k})$ of the incoming circularly polarized plane wave is contained in the YZ plane and forms an angle θ with the OZ axis perpendicular to the

https://dx.doi.org/10.1021/acsphotonics.0c00611
ACS Photonics XXXX, XXX, XXX−XXX

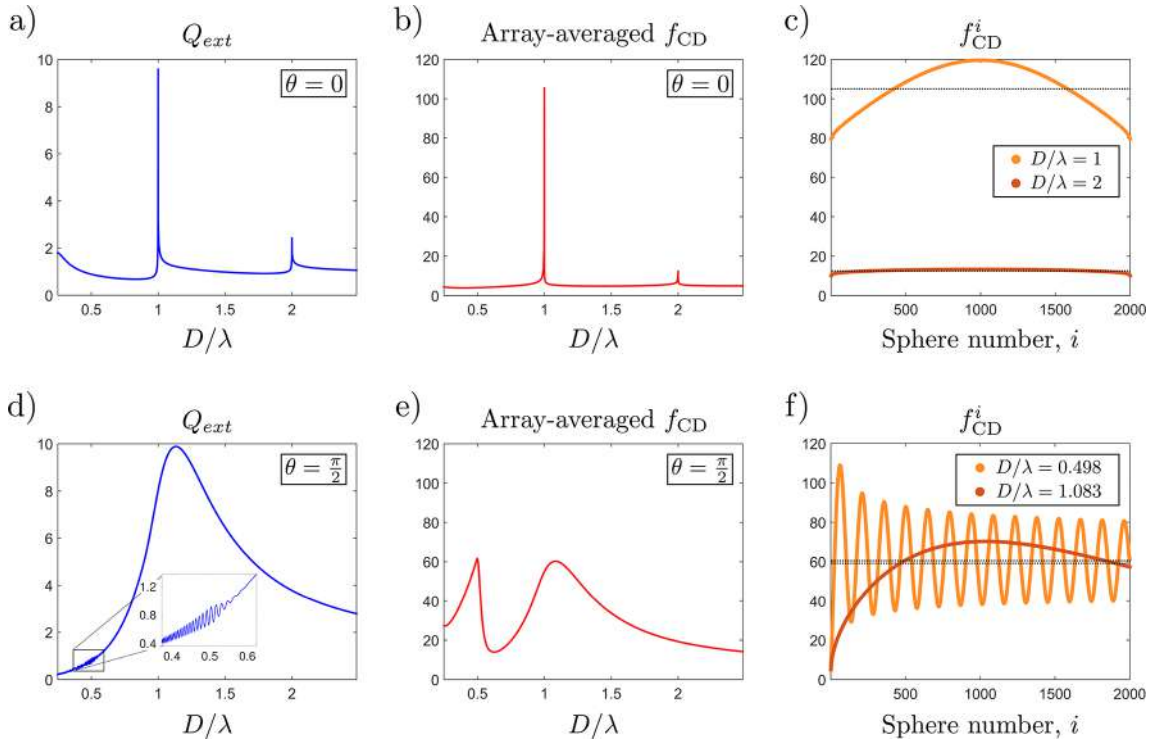

Figure 4. (a) Normalized extinction cross section and f_{CD} at Kerker's first condition ($\lambda = \lambda_k$) for normal and grazing incidence. (b) f_{CD}^{avg} for $\theta = 0$. (c) Distribution in the chain of the local CD enhancement factor at the two resonant conditions in (b). (d) Normalized extinction for an incidence of $\theta = \pi/2$. (e) f_{CD}^{avg} for $\theta = \pi/2$. (f) Distribution in the chain of the local CD enhancement factor at the two resonant conditions in (e). Black dotted line: average enhancement for the whole structure (f_{CD}^{avg}) at the resonant conditions in (b) and (e). The CD enhancement factor is calculated in (b) and (e) using eq 11, whereas in (c) and (f) the expression given by eq 10 is calculated for each sphere in the chain. In all the aforementioned, the integrand is calculated by making use of eq 3.

chain. A sketch of the parameters of the system can be seen in Figure 1.

To characterize the resonant features of the system, we first study the extinction cross section, C_{ext} of the particle chain. In this particular system, Kerker's first condition is exclusively fulfilled at $\lambda = \lambda_k = 1208$ nm, so we explore the extinction cross section of the system as a function of two parameters: the incidence angle, θ, and the interparticle distance, D. The results of this calculation are shown in Figure 2a, where the normalized extinction cross section, $Q_{ext} = C_{ext}/(N \cdot C_{ext,1})$, is shown and $C_{ext,1}$ is the extinction cross section of a single silicon particle at λ_k. Notice that the canonical limit for the validity of CDA is usually set within the condition $D > 3a$, that is, for interparticle distances, D, over three times the radius of the particles in the array.[43−46] Thus, in our system, the results for $D/\lambda \leq 0.37$ should be taken with some care. Nevertheless, all the interesting features we will focus on are found for $D/\lambda > 0.37$.

In Figure 2b, a comparison of our results with the extinction cross section of an infinite chain of particles is shown. For the infinite chain, in order to properly compare the cross sections to those of the finite chain, we define Q_{ext} as the extinction cross section per particle normalized to the extinction cross section of an isolated sphere (details of the theoretical formalism describing the infinite case[47,48] can be found in the Supporting Information). As expected, both calculations give very similar results since collective interactions are known to converge for a given number of elements in a periodic structure.[45,49] Interestingly, the number of nanospheres required in our system to reproduce the behavior of the infinite case at gracing incident angles is considerable comparing to the numbers found in the literature for low incident angles.[50,51]

The analytic calculations for the infinite chain allow us to identify the narrow peaks at low angles ($\theta \to 0$) as diffractive modes emerging close to Rayleigh anomalies,[51−54] given by $D/\lambda = m/(1 \pm k_y/k)$, where m takes positive integer values and k_y marks the periodicity of the field along the chain ($k_y/k = \sin\theta$). As stated above, these peaks emerge as a consequence of the constructive interference of far-field interactions. Figure 3 presents the extinction cross section of a single silicon sphere (Figure 3a) and chains of 2000 nanospheres for different interparticle distances as a function of incidence angle, θ, and wavelength, λ. Figure 3b reveals that chains of nanoparticles present narrow diffraction lines hybridized with the single-particle spectrum,[55] even at large interparticle distances.

However, Figure 2 presents an additional much wider resonance close to the grazing incidence ($\theta \to \pi/2$). This mode does not fit well with the diffractive characteristics and, thus, has to be interpreted in terms of a different interaction mechanism. Figure 3c,d unveils that this resonance emerges when particles in the chain are placed closer than $D = 1.5\lambda_k$. At those separation distances, near- and midfield contributions become important. As particles are placed closer together, the magnetic single-particle resonance of silicon ($\lambda_{mag} \sim 1110$ nm) redshifts and it can approach the wavelength of the Kerker condition, λ_k. All these considerations point out that this resonance is related to a bonding transversal mode of the chain, a configuration that has been extensively studied in nanoparticle dimers and metamaterials.[42]

https://dx.doi.org/10.1021/acsphotonics.0c00611
ACS Photonics XXXX, XXX, XXX−XXX

Moreover, at $\theta = \pi/2$, the complete physical configuration (incident wave included) is rotationally symmetric. Due to the simultaneous duality and axial symmetry, helicity can be expressed in this situation as

$$\Lambda = \frac{J_y P_y}{|P_y|} \tag{9}$$

where both J_y (y-component of the total angular momentum of light) and Λ are conserved quantities. Therefore, P_y (y-component of the linear momentum of light) cannot change signs under scattering and backward scattering is not allowed.[56] As a consequence, this mode is a forward propagating one.

Once we have thoroughly analyzed the optical resonances that can emerge in a dual 1D array of nanospheres, we proceed to show that, as predicted, all these resonances give rise to important enhancements of $f_{CD(\mathbf{r})}$. In order to model realistic environments of practical interest, we define two averaged enhancement factors: the average CD value around a particle at position $\mathbf{r}_i$ (f^i_{CD}) and the array-averaged CD enhancement factor (f^{avg}_{CD}) defined as

$$f^i_{CD} = \int_{S_i} \frac{1}{4\pi} f_{CD}(\xi, \eta) \sin\xi \, d\xi \, d\eta \tag{10}$$

$$f^{avg}_{CD} = \frac{1}{N} \sum_{i=1}^{N} f^i_{CD} \tag{11}$$

The integrals are carried out around a spherical surface S_i (ξ and η are, respectively, the polar and azimuthal spherical coordinates with respect to the center of the i-th nanoparticle) separated 1 nm apart from the surface of the i-th silicon nanoparticle.

Figure 4a presents the normalized extinction cross section of the silicon array as a function of the interparticle distance for $\theta = 0$. Under this incidence, the extinction shows a resonant behavior very close to the diffraction condition $D = m\lambda_k$, for $m \in \mathbb{N}$; however, the strength of the resonances decreases as m is increased. Previous works have shown that these resonances are quite robust against disorder, particularly against particle size disarrangement,[57,58] although resonances may occur at slightly different frequencies, and the maximum value of extinction may drop. In Figure 4b we can compare the extinction resonances with the CD enhancement averaged over the whole structure, f^{avg}_{CD}, for $\theta = 0$. We obtain 2 orders of magnitude CD enhancement (a factor of ∼110) averaged over the entire structure for the diffractive mode peaking close to $D/\lambda = 1$. Note that previous results[8] concluded that individual silicon nanoparticles of similar radii, were capable of inducing an enhancement of 1 order of magnitude in the molecular CD signal. Thus, this dual lattice design strategy provides an additional order of magnitude enhancement in f^{avg}_{CD}.

Also, the CD enhancement variation among the individual spheres of the chain is shown in Figure 4c. In this figure, we reflect the f^i_{CD} enhancement value around every sphere for the two resonant distances appearing in Figure 4b. The average values of the resonant enhancement for the whole structure (coinciding with the peak values of Figure 4b) are presented as a black dotted line. We can observe that both resonances have similar symmetric field distributions whose maximum is located right at the center of the array.

On the other hand, under incidence parallel to the array axis, at $\theta = \pi/2$, the normalized extinction cross section in Figure 4d shows a single broad peak around $D/\lambda \sim 1.1$. Analyzing the array-averaged CD enhancement factor, though two peaks are evident in Figure 4e, one at $D/\lambda \sim 1.1$ and another one around $D/\lambda \sim 0.5$, both showing maximum values of $f^{avg}_{CD} \sim 60$. As pointed out above, the f^{avg}_{CD} peak centered at $D/\lambda \sim 1.1$ is related to the red-shifted single-particle magnetic resonance, and thus, it is directly related to the peak in Figure 4d.

However, the second f^{avg}_{CD} peak at $D/\lambda \sim 0.5$ is not related to a prominent extinction peak, but with the small oscillations that the extinction shows at grazing angles (see inset in Figure 4d). These oscillations are not observed for the infinite case, which allows us to understand them as a finite size effect. As the angle of incidence increases, the end of the chain can provide the extra momentum necessary to couple to guided modes, that is, modes that lie beyond the light line (see Figure S1 in the Supporting Information), inaccessible for the infinite system. Since guided modes can only radiate energy at the chain ends, they can barely contribute to the extinction. Nonetheless, the coupling to guided modes concentrate the field around the chain, leading to strong near-fields[59] and providing large enhancements of f^{avg}_{CD}. This happens because these chain modes are typically characterized by sign-changing dipole distributions[60] whose contributions interfere destructively in the far-field. Figure 4f shows the spatial distribution of f^{avg}_{CD} in the chain for the two resonant conditions in Figure 4e. Note that for $D/\lambda = 0.498$, the $f_{CD(\mathbf{r})}$ distribution in Figure 4f (yellow line) represents a guided mode of the chain with a considerable propagation length.

Finally, it is remarkable that, after a monotonous growth, f^{avg}_{CD} drops off dramatically around $D/\lambda \sim 0.5$. In addition, the oscillations in the extinctions are no longer visible. All these features are connected to the dispersion relation of the modes supported by the chain. For $D/\lambda > 0.5$, modes can radiate energy due to the periodicity of the system (see Figure S1 in the Supporting Information). Therefore, guided modes become leaky, that is, modes that are not confined to the system. Then, energy is radiated out to the continuum and cannot be stored efficiently.

In conclusion, we have presented a systematic procedure to design periodic nanophotonic platforms capable of enhancing molecular CD spectroscopy resonantly. As an example, we applied the method to design a dual 1D periodic nanostructure made of high refractive index nanospheres. By analyzing the emergent collective features in the system, we have found that they can be classified in three different types: diffractive modes, nondiffractive modes, and finite chain effects. We have shown that far-field diffractive resonances can increase the array-averaged CD enhancement up to a factor of ∼110, providing an additional order of magnitude enhancement compared to the optical response of a single particle. Moreover, we find that nondiffractive modes and finite chain effects, which have not been previously considered in the surface-enhanced CD literature, also give rise to comparable enhancement magnitudes (over a factor of ∼60). Finally, the spherical symmetry of each of the lattice elements guarantees the conservation of helicity at all angles of incidence, permitting to enhance CD spectroscopy for any incoming wave direction. This method can be easily extended to more complicated platforms, such as 2D metasurfaces or 3D photonic crystals, opening venues to new designs and research directions.

https://dx.doi.org/10.1021/acsphotonics.0c00611
ACS Photonics XXXX, XXX, XXX−XXX

■ ASSOCIATED CONTENT

Supporting Information

The Supporting Information is available free of charge at https://pubs.acs.org/doi/10.1021/acsphotonics.0c00611.

General explanation of helicity conservation in composite systems, an in-depth explanation of the CDA formalism, both for a finite and an infinite array of nanoparticles with electric and magnetic dipolar responses, and detailed information on the relation of the extinction cross section under plane-wave illumination, with the analytical modes found for a dual 1D array of nanoparticles (PDF)

■ AUTHOR INFORMATION

Corresponding Authors

Jon Lasa-Alonso − *Centro de Física de Materiales (CSIC-UPV/EHU), 20018 Donostia-San Sebastian, Spain; Donostia International Physics Center, 20018 Donostia-San Sebastian, Spain*; Email: jlasa022@ikasle.ehu.eus

Aitzol García-Etxarri − *Donostia International Physics Center, 20018 Donostia-San Sebastian, Spain; IKERBASQUE, Basque Foundation for Science, 48013 Bilbao, Spain*; orcid.org/0000-0002-5867-2390; Email: aitzolgarcia@dipc.org

Authors

Diego Romero Abujetas − *Donostia International Physics Center, 20018 Donostia-San Sebastian, Spain; Instituto de Estructura de la Materia (CSIC), 28006 Madrid, Spain; Department of Materials Science and Engineering, Stanford University, Stanford, California 94305, United States*; orcid.org/0000-0002-6544-5305

Álvaro Nodar − *Centro de Física de Materiales (CSIC-UPV/EHU), 20018 Donostia-San Sebastian, Spain; Donostia International Physics Center, 20018 Donostia-San Sebastian, Spain*

Jennifer A. Dionne − *Department of Materials Science and Engineering, Stanford University, Stanford, California 94305, United States*; orcid.org/0000-0001-5287-4357

Juan José Sáenz − *Donostia International Physics Center, 20018 Donostia-San Sebastian, Spain; IKERBASQUE, Basque Foundation for Science, 48013 Bilbao, Spain*; orcid.org/0000-0002-1411-5648

Gabriel Molina-Terriza − *Centro de Física de Materiales (CSIC-UPV/EHU), 20018 Donostia-San Sebastian, Spain; Donostia International Physics Center, 20018 Donostia-San Sebastian, Spain; IKERBASQUE, Basque Foundation for Science, 48013 Bilbao, Spain*

Javier Aizpurua − *Centro de Física de Materiales (CSIC-UPV/EHU), 20018 Donostia-San Sebastian, Spain; Donostia International Physics Center, 20018 Donostia-San Sebastian, Spain*; orcid.org/0000-0002-1444-7589

Complete contact information is available at: https://pubs.acs.org/10.1021/acsphotonics.0c00611

Notes

The authors declare no competing financial interest.

■ ACKNOWLEDGMENTS

J.L.A., J.J.S., and A.G.E. acknowledge the PID2019-109905GA-C22 Project of the Spanish Ministerio de Ciencia, Innovacion y Universidades (MICIU). D.R.A. acknowledges partial financial support from Grant No. MELODIA PGC2018-095777-B-C21 of MICIU and from the Ministerio de Educación, Cultura y Deporte through the FPU Ph.D. Fellowship FPU15/03566. A.N. acknowledges finacial support from the MICIU through the FPI Ph.D. Fellowship BES-2017-080073. G.M.T. acknowledges the FIS2017-87363-P Project of the Spanish MINECO. A.G.E. and J.A. acknowledge the FIS2016-80174-P Project of the Spanish MINECO. A.G.E. received funding from the Gipuzkoako Foru Aldundia OF23/2019 (ES) Project, "Fellows Gipuzkoa" Fellowship through FEDER "Una Manera de hacer Europa", and by Eusko Jaurlaritza Grant Numbers KK-2017/00089, IT1164-19, PI2016-41, and KK-2019/00101.

■ DEDICATION

This manuscript is dedicated to the memory of Juan José Sáenz, Mole, beloved colleague, friend, and mentor of many, who deceased on March 22, 2020.

■ REFERENCES

(1) Barron, L. D. *Molecular Light Scattering and Optical Activity*, 2nd ed.; Cambridge University Press, 2004.

(2) Neubrech, F.; Pucci, A.; Cornelius, T. W.; Karim, S.; García-Etxarri, A.; Aizpurua, J. Resonant Plasmonic and Vibrational Coupling in a Tailored Nanoantenna for Infrared Detection. *Phys. Rev. Lett.* **2008**, *101*, 157403.

(3) Hartstein, A.; Kirtley, J. R.; Tsang, J. C. Enhancement of the Infrared Absorption from Molecular Monolayers with Thin Metal Overlayers. *Phys. Rev. Lett.* **1980**, *45*, 201−204.

(4) Stiles, P. L.; Dieringer, J. A.; Shah, N. C.; Van Duyne, R. P. Surface-Enhanced Raman Spectroscopy. *Annu. Rev. Anal. Chem.* **2008**, *1*, 601−626.

(5) Le Ru, E. C.; Blackie, E.; Meyer, M.; Etchegoin, P. G. Surface Enhanced Raman Scattering Enhancement Factors: A Comprehensive Study. *J. Phys. Chem. C* **2007**, *111*, 13794−13803.

(6) Ameer, F. S.; Hu, W.; Ansar, S. M.; Siriwardana, K.; Collier, W. E.; Zou, S.; Zhang, D. Robust and Reproducible Quantification of SERS Enhancement Factors Using a Combination of Time-Resolved Raman Spectroscopy and Solvent Internal Reference Method. *J. Phys. Chem. C* **2013**, *117*, 3483−3488.

(7) Tang, Y.; Cohen, A. E. Optical Chirality and Its Interaction with Matter. *Phys. Rev. Lett.* **2010**, *104*, 163901.

(8) García-Etxarri, A.; Dionne, J. A. Surface-enhanced circular dichroism spectroscopy mediated by nonchiral nanoantennas. *Phys. Rev. B: Condens. Matter Mater. Phys.* **2013**, *87*, 235409.

(9) Vestler, D.; Ben-Moshe, A.; Markovich, G. Enhancement of Circular Dichroism of a Chiral Material by Dielectric Nanospheres. *J. Phys. Chem. C* **2019**, *123*, 5017−5022.

(10) Ho, C.-S.; Garcia-Etxarri, A.; Zhao, Y.; Dionne, J. Enhancing Enantioselective Absorption Using Dielectric Nanospheres. *ACS Photonics* **2017**, *4*, 197−203.

(11) Raziman, T. V.; Godiksen, R. H.; Müller, M. A.; Curto, A. G. Conditions for Enhancing Chiral Nanophotonics near Achiral Nanoparticles. *ACS Photonics* **2019**, *6*, 2583−2589.

(12) Garcia-Etxarri, A.; Ugalde, J. M.; Saenz, J. J.; Mujica, V. Field-Mediated Chirality Information Transfer in Molecule-Nanoparticle Hybrids. *J. Phys. Chem. C* **2020**, *124*, 1560.

(13) Graf, F.; Feis, J.; Garcia-Santiago, X.; Wegener, M.; Rockstuhl, C.; Fernandez-Corbaton, I. Achiral, Helicity Preserving, and Resonant Structures for Enhanced Sensing of Chiral Molecules. *ACS Photonics* **2019**, *6*, 482−491.

(14) Schäferling, M.; Dregely, D.; Hentschel, M.; Giessen, H. Tailoring Enhanced Optical Chirality: Design Principles for Chiral Plasmonic Nanostructures. *Phys. Rev. X* **2012**, *2*, 031010.

(15) Nesterov, M. L.; Yin, X.; Schäferling, M.; Giessen, H.; Weiss, T. The Role of Plasmon-Generated Near Fields for Enhanced Circular Dichroism Spectroscopy. *ACS Photonics* **2016**, *3*, 578−583.

(16) Vestler, D.; Shishkin, I.; Gurvitz, E. A.; Nasir, M. E.; Ben-Moshe, A.; Slobozhanyuk, A. P.; Krasavin, A. V.; Levi-Belenkova, T.; Shalin, A. S.; Ginzburg, P.; Markovich, G.; Zayats, A. V. Circular dichroism enhancement in plasmonic nanorod metamaterials. *Opt. Express* **2018**, *26*, 17841−17848.
(17) Lee, S.; Yoo, S.; Park, Q.-H. Microscopic Origin of Surface-Enhanced Circular Dichroism. *ACS Photonics* **2017**, *4*, 2047−2052.
(18) Vázquez-Lozano, J. E.; Martínez, A. Towards Chiral Sensing and Spectroscopy Enabled by All-Dielectric Integrated Photonic Waveguides. *Laser Photonics Rev.* **2020**, *14*, 1900422.
(19) Solomon, M. L.; Hu, J.; Lawrence, M.; García-Etxarri, A.; Dionne, J. A. Enantiospecific Optical Enhancement of Chiral Sensing and Separation with Dielectric Metasurfaces. *ACS Photonics* **2019**, *6*, 43−49.
(20) Mohammadi, E.; Tsakmakidis, K. L.; Askarpour, A. N.; Dehkhoda, P.; Tavakoli, A.; Altug, H. Nanophotonic Platforms for Enhanced Chiral Sensing. *ACS Photonics* **2018**, *5*, 2669−2675.
(21) Garcia-Guirado, J.; Svedendahl, M.; Puigdollers, J.; Quidant, R. Enhanced chiral sensing with dielectric nano-resonators. *Nano Lett.* **2020**, *20*, 585−591.
(22) Hanifeh, M.; Capolino, F. Helicity maximization in a planar array of achiral high-density dielectric nanoparticles. *J. Appl. Phys.* **2020**, *127*, 093104.
(23) Fernandez-Corbaton, I.; Zambrana-Puyalto, X.; Tischler, N.; Vidal, X.; Juan, M. L.; Molina-Terriza, G. Electromagnetic Duality Symmetry and Helicity Conservation for the Macroscopic Maxwell's Equations. *Phys. Rev. Lett.* **2013**, *111*, 060401.
(24) Barnett, S. M.; Cameron, R. P.; Yao, A. M. Duplex symmetry and its relation to the conservation of optical helicity. *Phys. Rev. A: At., Mol., Opt. Phys.* **2012**, *86*, 013845.
(25) Cameron, R. P.; Barnett, S. M.; Yao, A. M. Optical helicity, optical spin and related quantities in electromagnetic theory. *New J. Phys.* **2012**, *14*, 053050.
(26) Nieto-Vesperinas, M. Chiral optical fields: a unified formulation of helicity scattered from particles and dichroism enhancement. *Philos. Trans. R. Soc., A* **2017**, *375*, 20160314.
(27) Poulikakos, L. V.; Dionne, J. A.; García-Etxarri, A. Optical Helicity and Optical Chirality in Free Space and in the Presence of Matter. *Symmetry* **2019**, *11*, 1113.
(28) Messiah, A. *Quantum Mechanics*; Dover Publications Inc., 1999.
(29) Zambrana-Puyalto, X.; Fernandez-Corbaton, I.; Juan, M.; Vidal, X.; Molina-Terriza, G. Duality symmetry and Kerker conditions. *Opt. Lett.* **2013**, *38*, 1857−1859.
(30) Schmidt, M. K.; Aizpurua, J.; Zambrana-Puyalto, X.; Vidal, X.; Molina-Terriza, G.; Sáenz, J. J. Isotropically Polarized Speckle Patterns. *Phys. Rev. Lett.* **2015**, *114*, 113902.
(31) Olmos-Trigo, J.; Sanz-Fernández, C.; Bergeret, F. S.; Sáenz, J. J. Asymmetry and spin-orbit coupling of light scattered from subwavelength particles. *Opt. Lett.* **2019**, *44*, 1762−1765.
(32) Nieto-Vesperinas, M.; Gomez-Medina, R.; Saenz, J. J. Angle-suppressed scattering and optical forces on submicrometer dielectric particles. *J. Opt. Soc. Am. A* **2011**, *28*, 54−60.
(33) Geffrin, J.-M.; García-Cámara, B.; Gómez-Medina, R.; Albella, P.; Froufe-Pérez, L.; Eyraud, C.; Litman, A.; Vaillon, R.; González, F.; Nieto-Vesperinas, M.; Sáenz, J.; Moreno, F. Magnetic and electric coherence in forward-and back-scattered electromagnetic waves by a single dielectric subwavelength sphere. *Nat. Commun.* **2012**, *3*, 1171.
(34) Garcia-Etxarri, A. Optical polarization mobius strips on all-dielectric optical scatterers. *ACS Photonics* **2017**, *4*, 1159−1164.
(35) Olmos-Trigo, J.; Sanz-Fernández, C.; García-Etxarri, A.; Molina-Terriza, G.; Bergeret, F. S.; Sáenz, J. J. Enhanced spin-orbit optical mirages from dual nanospheres. *Phys. Rev. A: At., Mol., Opt. Phys.* **2019**, *99*, 013852.
(36) Olmos-Trigo, J.; Abujetas, D. R.; Sanz-Fernandez, C.; Zambrana-Puyalto, X.; de Sousa, N.; Sanchez-Gil, J. A.; Saenz, J. J. Unveiling dipolar spectral regimes of large dielectric Mie spheres from helicity conservation. *Phys. Rev. Research* **2020**, *2*, na.
(37) García-Etxarri, A.; Gómez-Medina, R.; Froufe-Pérez, L. S.; López, C.; Chantada, L.; Scheffold, F.; Aizpurua, J.; Nieto-Vesperinas, M.; Sáenz, J. J. Strong magnetic response of submicron Silicon particles in the infrared. *Opt. Express* **2011**, *19*, 4815−4826.
(38) Bialynicki-Birula, I.; Bialynicka-Birula, Z. The role of the Riemann−Silberstein vector in classical and quantum theories of electromagnetism. *J. Phys. A: Math. Theor.* **2013**, *46*, 053001.
(39) Palik, E. D. *Handbook of Optical Constants of Solids*; Academic Press, 1998.
(40) Hicks, E. M.; Zou, S.; Schatz, G. C.; Spears, K. G.; Van Duyne, R. P.; Gunnarsson, L.; Rindzevicius, T.; Kasemo, B.; Käll, M. Controlling Plasmon Line Shapes through Diffractive Coupling in Linear Arrays of Cylindrical Nanoparticles Fabricated by Electron Beam Lithography. *Nano Lett.* **2005**, *5*, 1065−1070.
(41) Ross, M. B.; Mirkin, C. A.; Schatz, G. C. Optical Properties of One-, Two-, and Three-Dimensional Arrays of Plasmonic Nanostructures. *J. Phys. Chem. C* **2016**, *120*, 816−830.
(42) Halas, N. J.; Lal, S.; Chang, W.-S.; Link, S.; Nordlander, P. Plasmons in Strongly Coupled Metallic Nanostructures. *Chem. Rev.* **2011**, *111*, 3913−3961.
(43) Park, S. Y.; Stroud, D. Surface-plasmon dispersion relations in chains of metallic nanoparticles: An exact quasistatic calculation. *Phys. Rev. B: Condens. Matter Mater. Phys.* **2004**, *69*, 125418.
(44) Weber, W. H.; Ford, G. W. Propagation of optical excitations by dipolar interactions in metal nanoparticle chains. *Phys. Rev. B: Condens. Matter Mater. Phys.* **2004**, *70*, 125429.
(45) Citrin, D. S. Plasmon polaritons in finite-length metal-nanoparticle chains: the role of chain length unravelled. *Nano Lett.* **2005**, *5*, 985−989.
(46) Evlyukhin, A. B.; Reinhardt, C.; Seidel, A.; Luk'yanchuk, B. S.; Chichkov, B. N. Optical response features of Si-nanoparticle arrays. *Phys. Rev. B: Condens. Matter Mater. Phys.* **2010**, *82*, 045404.
(47) Maximon, L. C. The dilogarithm function for complex argument. *Proc. R. Soc. London, Ser. A* **2003**, *459*, 2807−2819.
(48) Shore, R. A.; Yaghjian, A. D. Complex waves on periodic arrays of lossy and lossless permeable spheres: 1. Theory. *Radio Sci.* **2012**, *47*, 1−16.
(49) Rodriguez, S.R.K.; Schaafsma, M.C.; Berrier, A.; Gomez Rivas, J. Collective resonances in plasmonic crystals: Size matters. *Phys. B* **2012**, *407*, 4081−4085. Proceedings of the conference - Wave Propagation: From Electrons to Photonic Crystals and Metamaterials.
(50) Rodriguez, S.; Schaafsma, M.; Berrier, A.; Gomez Rivas, J. Collective resonances in plasmonic crystals: Size matters. *Phys. B* **2012**, *407*, 4081−4085.
(51) Kravets, V. G.; Kabashin, A. V.; Barnes, W. L.; Grigorenko, A. N. Plasmonic Surface Lattice Resonances: A Review of Properties and Applications. *Chem. Rev.* **2018**, *118*, 5912−5951.
(52) Zou, S.; Janel, N.; Schatz, G. C. Silver nanoparticle array structures that produce remarkably narrow plasmon lineshapes. *J. Chem. Phys.* **2004**, *120*, 10871−10875.
(53) García de Abajo, F. J.; Sáenz, J. J. Electromagnetic Surface Modes in Structured Perfect-Conductor Surfaces. *Phys. Rev. Lett.* **2005**, *95*, 233901.
(54) Vecchi, G.; Giannini, V.; Gómez Rivas, J. Surface modes in plasmonic crystals induced by diffractive coupling of nanoantennas. *Phys. Rev. B: Condens. Matter Mater. Phys.* **2009**, *80*, 201401.
(55) Utyushev, A. D.; Zakomirnyi, V. I.; Ershov, A. E.; Gerasimov, V. S.; Karpov, S. V.; Rasskazov, I. L. Collective Lattice Resonances in All-Dielectric Nanostructures under Oblique Incidence. *Photonics* **2020**, *7*, 24.
(56) Kerker, M.; Wang, D.-S.; Giles, C. L. Electromagnetic scattering by magnetic spheres. *J. Opt. Soc. Am.* **1983**, *73*, 765−767.
(57) Prasad, T.; Colvin, V. L.; Mittleman, D. M. The effect of structural disorder on guided resonances in photonic crystal slabs studied with terahertz time-domain spectroscopy. *Opt. Express* **2007**, *15*, 16954−16965.
(58) Auguié, B.; Barnes, W. L. Diffractive coupling in gold nanoparticle arrays and the effect of disorder. *Opt. Lett.* **2009**, *34*, 401−403.

https://dx.doi.org/10.1021/acsphotonics.0c00611
ACS Photonics XXXX, XXX, XXX−XXX

(59) Liu, M.; Lee, T.-W.; Gray, S. K.; Guyot-Sionnest, P.; Pelton, M. Excitation of Dark Plasmons in Metal Nanoparticles by a Localized Emitter. *Phys. Rev. Lett.* **2009**, *102*, 107401.
(60) Weber, W. H.; Ford, G. W. Propagation of optical excitations by dipolar interactions in metal nanoparticle chains. *Phys. Rev. B: Condens. Matter Mater. Phys.* **2004**, *70*, 125429.

https://dx.doi.org/10.1021/acsphotonics.0c00611
ACS Photonics XXXX, XXX, XXX−XXX